PAPER

Check for updates

Microwave-assisted synthesis of copper-loaded polyamidoxime brushes as an efficient catalytic system for nitroarene reduction†

Shaista Taimur, [iD] ‡*[a] Shajia Rehman,‡[a] Mujtaba Ellahi,[b] Syed Rizwan, [iD] [c] Humaira Razzaq [iD] [a] and Tariq Yasin[d]

This study reports the development of copper-loaded polyamidoxime polymer brushes (Cu-AO-PB) as a heterogeneous catalyst *via* microwave-assisted graft polymerization for the first time. Microwave-assisted synthesis allows faster and more uniform heating, leading to shorter reaction times, more energy-efficiency and better control over catalyst morphology reducing production costs and environmental impact. In contrast to the traditional methods, catalysts prepared using microwave techniques often demonstrate superior activity and selectivity due to their unique structural characteristics. The influence of different parameters on the grafting of acrylonitrile onto vinyl sepiolite was studied and a maximum of 449% grafting-percentage was obtained with 89% grafting-efficiency. Polyacrylonitrile grafted brushes were chemically modified to polyamidoxime followed by copper complexation. The surface morphology and chemical composition of the synthesized polymer brushes were assessed by SEM, TEM, XRD, TGA and FTIR. The catalytic capability of Cu-AO-PB was assessed systematically for 4-nitrophenol to 4-aminophenol reduction utilizing a UV-visible spectrophotometer. The Langmuir–Hinshelwood model was exploited to study the mechanism of 4-nitrophenol reduction catalyzed by copper-loaded amidoxime-nanoclay polymer brushes. Thermodynamic studies revealed important insights about ΔG, ΔH and ΔS values. Turnover frequency (TOF) was calculated to be 1.65×10^{10} molecules g^{-1} s^{-1}. Due to the integrated synergy between Cu and the unique polyamidoxime-nanoclay support, Cu-AO-PB demonstrated elevated catalytic efficacy for nitroarene reduction achieving a significantly higher reaction rate (0.0143 s^{-1}) and lower activation energy (28 kJ mol^{-1}) within 360 s.

1. Introduction

Polymer brushes have gathered significant attention in recent years driven by their diverse applications in catalysis, optoelectronics, drug delivery, medical diagnosis and much more.[1] They are macromolecular structures with polymer chains

[a] *Department of Chemistry, University of Wah, Quaid Avenue, Wah 47040, Pakistan. E-mail: shaista.taimur@uow.edu.pk, shajiarehman38@gmail.com, humaira.razzaq@uow.edu.pk*

[b] *Department of Chemistry, Balochistan University of Information Technology, Engineering and Management Sciences (BUITEMS), Quetta 87100, Pakistan. E-mail: mujtaba.ellahi@gmail.com*

[c] *Physics Characterization and Simulation Lab (PCSL), Department of Physics, School of Natural Sciences (SNS), National University of Sciences and Technology (NUST), Islamabad 44000, Pakistan. E-mail: syedrizwanh83@gmail.com*

[d] *Department of Chemistry, Pakistan Institute of Engineering and Applied Sciences, Nilore, Islamabad 44000, Pakistan. E-mail: yasintariq@gmail.com*

† Electronic supplementary information (ESI) available. See DOI: https://doi.org/10.1039/d4ma00763h

‡ These authors have contributed equally to this work and are co-first authors.

densely tethered to a substrate, resulting in a dense and conformal layer resembling the bristles of a brush.[2] Grafting of functional polymer chains onto the surface of a planar, spherical or cylindrical matrix can remarkably alter the surface properties of the matrix as well as provide new hybrid materials with improved properties.[3] As reported by Data Bridge Market Research, the polymer brushes market will reach an estimated value of 158.42 million dollars by 2028 and grow at a rate of 5.12% for the forecast period of 2021 to 2028. From the last few decades, a greener approach for the synthesis of polymeric materials has garnered attention minimizing environmental concerns.[4] The development of innovative approaches for utilizing environmentally benign methods is highly demanding. Numerous polymerization techniques have been developed to meet the demand of producing high-quality, economical, and eco-friendly polymeric materials.[5] The microwave-assisted graft polymerization (MAGP) offers swift and efficient heating significantly reducing the reaction time from hours to minutes, curtailing energy consumption and enhancing product purity

and yield.[6,7] Microwaves are non-ionizing electromagnetic radiations with wavelength ranging from 1 mm–30 cm and frequency between 300 MHz–300 GHz and energy of 2×10^{-24} J.[8] Microwaves provide dielectric heating by penetrating materials and heating up internal moisture.[9] In the past few years, novel auxiliary strategies have been investigated to improve not only the catalyst development but also catalytic reactions. The external fields like microwave-assisted and current-assisted catalysis have been explored for their potential in refining the performance and efficiency of the catalyst. Microwave-assisted graft polymerization has been utilized to enhance the reaction kinetics for better dispersion of active catalytic sites with uniform heating, which in turn promotes catalytic activity. Likewise, the current-assisted synthesis can persuade surface polarization facilitating electron transfer and enhancing catalytic activity and selectivity.[10] New avenues can be provided by integrating these promising auxiliary approaches for fabricating stable and selective catalysts. Conventional heating methods take hours and even days to complete the reaction, whereas microwaves accomplish the same within a few minutes, highlighting its energy-saving approach. Polymer brushes synthesized *via* MAGP involve the covalent attachment of polymer chains onto a substrate by using microwaves.[11] The MAGP epitomizes a substantial advancement in synthetic chemistry, contributing fast, effective, and environmentally friendly replacements to conventional heating methods for wide-ranging chemical transformations. A comparison of conventional heating methods with the microwave heating method is presented in Table S1 (ESI†).

Polyamidoxime, a polymer characterized by the presence of an oxime functional group, demonstrates remarkable efficacy in metal ion binding due to its inherent chelation capabilities, making polyamidoxime an exceptional adsorbent. One notable application of this polymer lies in its efficient extraction of uranium from seawater, a process crucial for securing uranium resources.[12] Polyamidoxime demonstrates selectivity for the adsorption of copper.[13] The incorporation of polyamidoxime brushes onto sepiolite nanoclay can make a good synergy to enhance the adsorption performance. Sepiolite is a naturally occurring hydrated magnesium silicate with molecular formula $Mg_4Si_6O_{15}(OH)_2 \cdot 6H_2O$. It has unique structural and morphological properties that make it an excellent candidate for serving as a substrate for polymer brush synthesis. The structural uniqueness of this nanofibrous clay lies in the availability of silanol groups (2.5 Si–OH groups per nm^2) on its surface, which offer the execution of different modification routes.[14] Utilizing sepiolite not only provides cost-effectiveness, but also offers various benefits such as high surface area and porosity, low toxicity and high thermal stability.[15] In the case of sepiolite-supported polymer brushes, polymer chains extend in all directions due to the nanofibrous nature of sepiolite.

4-Nitrophenol (4-NP) is incorporated into the environment through anthropogenic activities such as production of drugs like acetaminophen and phenetidine, pesticides like methyl and ethyl parathion, dyes to darken leather and military applications.[16] The US Environmental Protection Agency

ranked 4-NP as one of the topmost 114 organic contaminants owing to its widespread utilization leading to contamination of industrial wastewater streams related to its preparation, distribution and application.[17] According to studies, the acute toxicity of 4-NP to aquatic organisms is alarming, with reported LC50 values as low as 0.11 mg L^{-1} for fish species.[18] The acute exposure of 4-NP can cause methemoglobin formation resulting in blood related disorders, kidney and liver malfunction, eye and skin irritation, and anemia.[19] The toxic nature of 4-NP highlights the importance of developing eco-friendly and sustainable reduction methods. 4-NP reduction to 4-aminophenol (4-AP) is a crucial organic transformation that requires the use of a suitable catalyst to enhance the reaction efficiency.[20] In this context, heterogeneous catalysts offer notable advantages over homogeneous catalysts. Heterogeneous catalysts provide enhanced recyclability, ease of separation, and reduced environmental impact. These catalysts, when immobilized on solid supports, facilitate efficient reaction pathways, minimizing the release of toxic byproducts. As the environment strives for greener chemical processes, the adoption of heterogeneous catalysts in the reduction of 4-NP becomes a pivotal step towards sustainable and environmentally conscious practices in organic synthesis.

Herein, we report a novel and reliable method for the development of a polymer brush catalytic system *via* MAGP. After functionalization of sepiolite (SP) by vinyl triethoxysilane (VTES), acrylonitrile monomer was grafted onto a vinyl-modified sepiolite substrate (VS) using microwave radiations. Traditional heating methods are time-extensive, while MAGP offers a swift and energy efficient alternative with good control over polymerization, minimum reaction time and maximum product yield.[21] The grafted polyacrylonitrile nanohybrid polymer brushes were chemically transformed to polyamidoxime functional groups. After loading polyamidoxime polymer brush with copper (Cu-AO-PB), the catalytic proficiency of the developed material was demonstrated through a model reaction involving 4-NP reduction to 4-AP. Usually expensive metals like gold, platinum, *etc* are used for complexation with some suitable adsorbent material, and copper being relatively inexpensive is being utilized for complexation with polyamidoxime polymer brushes as a catalyst for the first time to the best of our knowledge. Moreover, the use of a green solvent enhances the method's sustainability. This innovative synthesis approach, combined with the unique properties of sepiolite as a substrate, offer a potent and environmentally friendly catalyst suitable for a variety of chemical synthesis applications.

2. Experimental

2.1. Materials and chemicals

Sepiolite, vinyl-triethoxysilane (VTES 97%), acrylonitrile (99%), hydrochloric acid (37%), methanol (99%), acetone (99%), dimethylformamide (DMF, 98%), hydroxylamine hydrochloride (98%), potassium per sulphate (KPS, 99%), copper sulphate pentahydrate ($CuSO_4 \cdot 5H_2O$, 98%), 4-nitrophenol (4-NP, 99%)

and sodium borohydride (NaBH4, 98%) were procured from Sigma Aldrich, and anhydrous sodium carbonate (99.5%) from Honeywell, whereas isopropanol (C_3H_8O, 99.5%) from Daejung. All chemicals were used without further purification as they are of analytical grade.

2.2. Synthesis

2.2.1. Vinyl functionalization of sepiolite and microwave-assisted graft polymerization of acrylonitrile onto vinyl-modified sepiolite. Sepiolite was modified according to a reported method. 10 g pristine sepiolite (PS) was dissolved in 1 L distilled water, then it was supplemented with 1 ml of 0.5 M HCl solution and kept stirring for 24 hrs. Then it was filtered and dried resulting in purified and acidified sepiolite (PAS). After that, it was dispersed in 333 ml isopropanol and 22.1 ml hydrolyzed VTES was introduced drop-wise and the solution was agitated for 3 h at 65 °C. This vinyl modified sepiolite (VS) was washed with methanol and then dried at 50 °C until constant weight.

2 g VS and 2 g Tween-80 were introduced into 20 ml distilled water in a nitrogen purged glass reactor. After agitation for 5 min, 10 g of acrylonitrile monomer was introduced. It was further stirred for 30 min, and subsequently 1 g of KPS was added as initiator and stirred again for 3 min. Then this glass reactor was placed in a domestic microwave oven (DW-MD5-S). After 3 min, the washing of the polymer brush first with distilled water and then with acetone was carried out three times. To completely remove the homopolymer from the reaction mixture, Soxhlet extraction was performed using DMF for 8 hours at 30 °C[22] and then vacuum dried at 50 °C until constant weight. The developed product was coded as acrylonitrile polymer brush (AN-PB). The grafting percentage (*G*%) and efficiency (GE%) were calculated as follows:

$$G\% = \frac{W_{\text{AN-PB}} - W_{\text{VS}}}{W_{\text{VS}}} \times 100 \qquad (1)$$

$$\text{GE}\% = \frac{W_{\text{AN-PB}} - W_{\text{VS}}}{W_{\text{AN}}} \times 100 \qquad (2)$$

where $W_{\text{AN-PB}}$ and W_{VS} are the weights of grafted and ungrafted VS and W_{AN} is the weight of the monomer.

2.2.2. Functional group modification of the polymer brush to amidoxime. The nitrile group of AN-PB was chemically modified into an amidoxime group by the following procedure. 1 g AN-PB and 10 g hydroxylamine hydrochloride were incorporated in a 1:1 mixture of water and methanol followed by the addition of 7.5 g of anhydrous sodium carbonate. The solution's pH was monitored and maintained at 7. The mixture was refluxed with stirring at 80 °C for 6 hrs. A color change was observed from cream to light pink during the course of the reaction. After filtration, amidoxime polymer brush (AO-PB) was washed thrice with distilled water and vacuum dried at 60 °C. The following formulae were used to determine the group density of AO (AO-GD) and conversion ratio of nitrile to

amidoxime (AO%):[23]

$$\text{AO-GD} \ (\text{mmol g}^{-1}) = \frac{W_{\text{AO-PB}} - W_{\text{AN-PB}}/33}{W_{\text{AO-PB}}} \times 1000 \qquad (3)$$

$$\text{AO}\% = \frac{W_{\text{AO-PB}} - W_{\text{AN-PB}}/33}{W_{\text{AN-PB}} - W_{\text{VS}}/53} \times 100 \qquad (4)$$

where $W_{\text{AO-PB}}$, $W_{\text{AN-PB}}$ and W_{VS} are the weights of AO-PB, AN-PB and VS, respectively. The molecular mass of hydroxylamine is 33 g mol^{-1} and acrylonitrile is 53 g mol^{-1}, respectively.

2.2.3. Copper complexation with amidoxime polymer brush (Cu-AO-PB). AO-PB (0.5 g) was dispersed in 50 ml of 1000 mg L^{-1} of Cu(II) prepared by using the analytical grade hydrated $CuSO_4$ solution. The color change of AO-PB was observed from pinkish to deep dark green indicating copper loading on AO-PB *via* complexation. For quantitative analysis, the adsorption capacity of the developed PBs for copper was determined by using an atomic absorption spectrophotometer (SpectrAA.300 plus, Varianuble beam). The Cu(II) ions adsorbed onto AO-PB (mg g^{-1}) at equilibrium were computed using eqn (5):

$$Q = \frac{(C_0 - C_e)V}{m} \qquad (5)$$

Here C_0 is the initial and C_e is the equilibrium concentration, V represents the volume (mL) of copper solution and m (mg) represents the mass of the AO-PB. The adsorption capacity was determined to be 291 mg g^{-1} which is in accordance with our previous work.[22] In this novel study, we report the use of copper-loaded polymer brushes (Cu-AO-PB) as a heterogeneous catalyst in subsequent experiments.

2.3. Characterizations

The FTIR spectra of the synthesized nanohybrid materials were acquired by using a PerkinElmer Spectrum 100 FTIR spectrophotometer. To ensure optimal signal-to-noise ratio, 100 scans per sample were conducted. Polymerization of acrylonitrile was carried out by using a domestic microwave oven DW-MD5-S. The thermal stability and degradation behavior of the developed nanocomposites were evaluated using a Mettler–Toledo thermogravimetric analyzer (TGA) subjecting 10 mg of sample to ambient to 800 °C temperature at the heating rate of 10 °C min^{-1} under a nitrogen atmosphere. X-Ray diffraction analyses were carried out at room temperature using a DRON-8 Bourevestnic diffractometer and data was collected over a 2θ range of 5° to 78° at a rate of 1.1 min^{-1}. The surface morphology alterations in the prepared samples were explored through TESCAN MIRA-3 field emission scanning electron microscopy coupled with an energy-dispersive X-ray (EDX) detector for elemental analysis. Structural changes in the modified sepiolite were investigated by using a transmission electron microscope, a Jeol JEM-2000FXII operating at 190 kV with a tungsten filament. Additionally, a SPECORD 200 PLUS 223E1156F UV-VIS spectrophotometer was employed for catalytic degradation of 4-NP to 4-AP.

2.4. Catalytic study

For evaluating the efficiency of Cu-AO-PB as a catalyst, 4-NP reduction to 4-AP was selected as an archetypal reaction. The

between copper ions and the nitrogen and oxygen atoms of the amidoxime group (Scheme S1, ESI†).[27]

3.1. Effect of reaction parameters on acrylonitrile grafting by microwave irradiations

In general, the $G\%$ is effected by a number of factors, such as extent of surface modification of sepiolite, exposure time, concentration of monomer, initiator, surfactant and microwave irradiation power. These parameters were investigated as follows.

3.1.1. Effect of substrate dose. Fig. 1(A) indicates the effect of substrate on $G\%$ by varying the VS dose from 0.5 g to 2.5 g by keeping other parameters constant. Increasing the amount of VS up to 2 g significantly enhanced the grafting percentage due to the availability of surface sites on VS, promoting effective grafting reaction. Beyond this point, further increase in VS leads to steric hindrance, limited monomer access to grafting sites and thus decreasing grafting phenomenon. Chaudhari *et al.* observed the same phenomenon of decreased $G\%$ beyond an optimal point.[28]

3.1.2. Effect of exposure time. Fig. 1(B) shows the influence of contact time on $G\%$ of AN-PB under microwave irradiations. There was an initial increase in $G\%$, as the exposure time increased from 60 s to 180 s and it then levelled off. This initial increase was due to greater availability of energy, resulting in greater generation of free radicals.[29] The decrease in $G\%$ after 180 s was due to the decomposition of the polymer chains. Conventional heating methods require several hours to complete this reaction,[30] while the use of microwave irradiation has been demonstrated to markedly shorten the required reaction time (180 seconds only) for grafting. So MAGP proves to be an efficient graft polymerization method radically reducing the reaction time in contrast to conventional heating systems.

3.1.3. Effect of acrylonitrile monomer concentration. In this study, the acrylonitrile monomer concentration was increased gradually by keeping other parameters constant and the results are shown in Fig. 1(C). $G\%$ increased linearly by increasing acrylonitrile concentration and reached its maximum of 449% and 89% GE with 1 : 5 (VS to AN ratio) as the optimal condition. Initially, the low acrylonitrile concentration (lower than 1 : 5) results in low grafting percentage due to the non-availability of sufficient monomer against more grafting sites.[31] While at higher concentration of acrylonitrile (higher than 1 : 5), excess monomer can lead to a rapid and uncontrolled polymerization reaction, causing steric hindrance as the growing polymer chains interfere with each other.[32] This hindrance can make it challenging for the monomers to effectively graft on the substrate. Homopolymer formation is also responsible for this decline, where acrylonitrile molecules polymerize with each other forming PAN, without the desired grafting onto the substrate. Therefore, 1 : 5 is the most favorable ratio for achieving maximum grafting on the VS substrate.

3.1.4. Effect of initiator concentration. The initiator is a substance that initiates the formation of free radicals, which triggers the polymerization reaction by providing the energy to break the chemical bonds in monomer molecules.[33] Grafting of
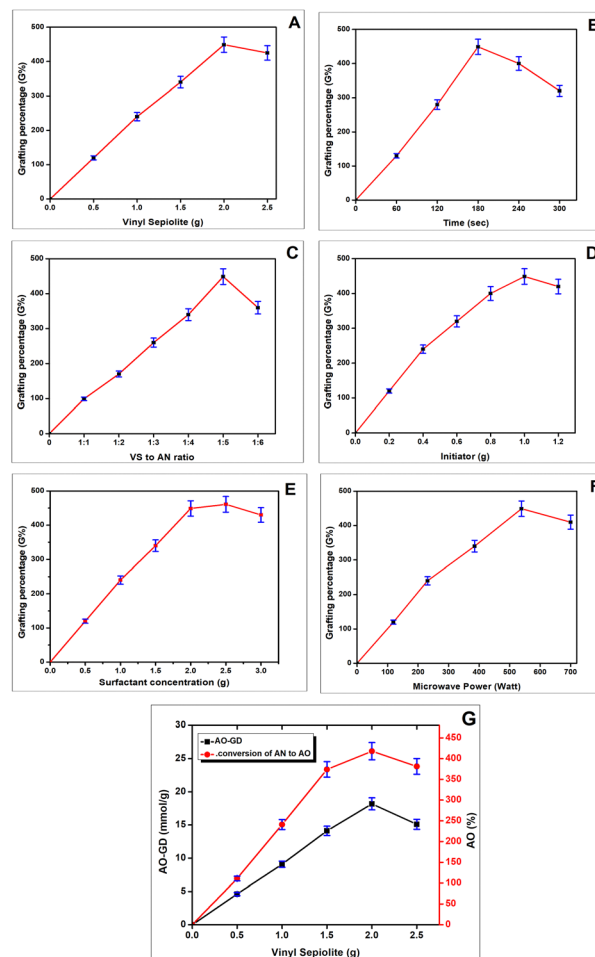

Fig. 1 Effect of different reaction parameters on grafting percentage of AN-PB onto VS. (A) Effect of substrate on $G\%$, (B) effect of exposure time on $G\%$, (C) effect of VS to AN ratio on $G\%$, (D) effect of initiator on $G\%$, (E) effect of surfactant on $G\%$, (F) effect of microwave irradiation power on $G\%$, and (G) effect of VS on AO-GD and AO%.

acrylonitrile onto VS was studied by varying the amount of initiator (KPS) from 0.2 g to 1.2 g. Fig. 1(D) indicates that by increasing the KPS concentration up to 1 g a sharp increase in $G\%$ was observed. After that, further enhancement in KPS concentration results in a decline in grafting percentage. Higher concentration of KPS encourages the formation of homopolymer, which leads to greater bulk viscosity restricting the diffusion of acrylonitrile monomer to the active grafting sites. The highest $G\%$ was achieved with 1 g of KPS.

3.1.5. Effect of surfactant concentration. Polysorbate 80 plays a vital role as a surfactant in graft polymerization by promoting stable colloidal dispersion and facilitating micelle formation leading to an enhanced grafting percentage.[34] Fig. 1(E) shows the effect of varying surfactant concentration from 0.5 to 3 g. Increasing surfactant concentration significantly enhanced the grafting percentage by facilitating monomer accessibility and reducing side reactions. Fig. 1(E) indicates a gradual increase in grafting percentage up to a surfactant concentration of 2 g. However, at higher

concentrations a decline in grafting percentage is observed. This decrease can be attributed to the formation of greater micelle population.[22] Maintaining the surfactant concentration below this optimal level ensures that the majority of surfactant molecules are available for grafting, resulting in a higher grafting percentage. Furthermore, the surfactant helps in preventing agglomeration of the grafted particles.[35]

3.1.6. Effect of microwave irradiation power. By varying the power of microwave radiation, it was observed that power directly influences the heating rate of the reaction mixture. As microwave radiations rotate the acrylonitrile molecules leading to lengthening its C–C double bond and causing the pi bond electron cloud to split up into two localized clouds, it results in the formation of free radical sites on carbon atoms. In order to synthesize AN-PB, the free radical sites of VS interact with those on acrylonitrile through a free radical reaction mechanism. Samples were subjected to different doses of MW exposure (120, 235, 385, 540 and 700 W). Fig. 1(F) shows that at 540 W, the highest grafting percentage was obtained. The initial increase in grafting percentage is due to greater availability of energy and monomer that results in the generation of more radicals. After 540 W, further increase in power results in a decrease in grafting percentage due to degradation of the resulting polymer and occurrence of side reactions.[36] Comparison of acrylonitrile $G\%$ with different reported substrates utilizing a domestic microwave oven is presented in Table 1. Research conducted by Halmagyi et al. indicates that low-power microwave irradiation produces negligible thermal effects over short exposure periods, whereas high-power microwave irradiation can lead to significant thermal increases, affecting polymer stability. For instance, it has been shown that low power microwaves can be performed effectively with power densities below 10 μW m^{-2}, allowing for longer exposure times without damaging the material.[37] Furthermore, Breugel et al. demonstrated in his study that the decomposition threshold of the polymers varies significantly with the power levels. For example, at lower power settings (e.g., 70 W), the exposure time required to reach the decomposition threshold can be substantially longer compared to higher power settings (e.g., 700 W). This highlights the necessity of adjusting exposure times based on the chosen power levels.[38]

3.1.7. Amidoxime group density (AO-GD) and amidoxime percentage (AO%). Polyacrylonitrile grafted polymer brushes were chemically modified into polyamidoxime. The AO-GD and AO (%) were calculated according to eqn (3) and (4) and the results are presented in Fig. 1(G). AO-GD basically refers to the

number of amidoxime groups present per gram of polyamidoxime and AO% refers to the number of nitrile groups converted into amidoxime. In this study, a maximum of 16 mmol g^{-1} AO-GD is obtained with 414 AO%, which is fairly in correspondence with the results of $G\%$ and quite encouraging as compared to the literature. Ghonamy et al. investigated the influence of grafted antioxidant on the attributes of acrylonitrile–butadiene copolymer and reported AO-GD of 0.15 mmol g^{-1} with 70 AO%.[44]

3.2. Composition study

FTIR spectra of PS and all its modified forms are revealed in Fig. 2. The FTIR spectrum of PS (Fig. 2(A)) demonstrates a medium intensity OH asymmetric and symmetric stretching vibration ranging from 3691 cm^{-1} to 3414 cm^{-1}. The Si–O–Mg band appears at 638 cm^{-1}. Stretching vibration of Si–O appears at 1017 cm^{-1}, its bending vibrations appear at 645, 784 and 979 cm^{-1} and Si–O–Si vibration appears at 1101 cm^{-1}.[45]

Fig. 2(B) displays the FTIR spectrum of PAS demonstrating the enhancement in intensity of some vibrations due to acid activation.[46] The FTIR spectrum of VS is shown in Fig. 2(C) indicating the augmentation of vibration at 1661 cm^{-1} owing to C=C stretch. A small vibration at 1397 is due to C–H bending and a band at 2971 cm^{-1} to 2900 cm^{-1} is ascribed to asymmetric and symmetric stretching vibrations of C–H bonds.[47] The increase in OH stretching vibration (Fig. 2(C)) is associated with the successful surface modification of PAS with VTES, as OH groups endorse the interfacial collaboration of sepiolite in organic solvents and polymers, which can enhance the thermomechanical behavior of the resulting composites.[48] The FTIR spectrum of AN-PB is displayed in Fig. 2(D). A new vibration at 2242 cm^{-1} is attributed to symmetrical stretch of the nitrile group[49] indicating the successful formation of polymer brushes with acrylonitrile chains grafted onto VS. The presence of the CH$_2$ group is established by the bending vibration at 1450 cm^{-1} whereas aliphatic C–H bonds in the polymer chain were demonstrated at 2930 cm^{-1}. In the FTIR spectrum of AO-PB (Fig. 2(E)) the dissipation of vibration at 2241 cm^{-1} and generation of some new peaks indicate successful modification of a nitrile group into amidoxime. New vibrations at 1207 cm^{-1}, 1382 cm^{-1} and 1645 cm^{-1} are credited for N–O, C–N and C=N groups of amidoxime, respectively, along with O–H and N–H stretch at 3100–3500 cm^{-1}.[50] In the FT-IR spectrum of

Table 1 Comparison of AN grafting by microwave irradiations on different substrates

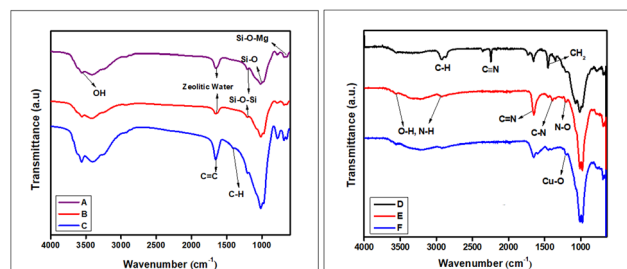| Substrate	$G\%$	References
Vinyl sepiolite	449	This study
Cassia siamea seed gum	80	39
Chitosan	105	40
Alumina	186	41
Psyllium mucilage chain	86	42
Starch	225	43

Fig. 2 FT-IR spectrum of PS (A), PAS (B), VS (C), AN-PB (D), AO-PB (E) and Cu-AO-PB (F).

Cu–AO-PB (Fig. 2(F)), the N–O band becomes less intense due to copper chelation with amidoxime by complexation. A small vibration appears at 1201 cm^{-1} attributed to Cu–O vibration. These findings helped in determining the copper–amidoxime complex in Scheme S1 (ESI†).

3.3. Thermal properties

TGA is a thermal study technique for the investigation of the stability of developed materials by gauging their weight variations as a function of temperature. The thermogram of SP (Fig. 3(a)-A) displays only 3% weight loss from 77–150 °C due to loss of moisture and adsorbed impurities. VS is likely to exhibit changes in its thermal behavior due to the presence of a vinyl group on the sepiolite surface. The thermogram of VS (Fig. 3(a)-B) demonstrates its weight loss in three steps. First 4% weight loss occurred from 83–210 °C which indicates loss of moisture and degradation of vinyl groups. Second 6% weight loss from 393–599 °C is due to complete decomposition of the organic content of VS.[51] While the third weight loss of 7% from 747–848 °C is due to the thermal decomposition of the sample.

The thermogram of AN-PB (Fig. 3(a)-C) manifests the thermal behavior of the developed polymer brushes. The first stage shows a 10% weight loss from 310–381 °C, which indicates the onset of polymer decomposition. In the second stage, a gradual weight loss from 540–780 °C occurred due to complete volatilization of the nitrile groups. TGA results were utilized to demonstrate the quantitative insight into the extent of the acrylonitrile polymer brush grafting process which were chemically attached to the VS surface. The amount of acrylonitrile grafted onto VS by MAGP was determined from the difference of residual weight loss using eqn (8).

$$\text{Acrylonitrile (meq g}^{-1}) = 10^3 \frac{(W_{200-800})}{(100 - W_{200-800})M_{AN}} \quad (8)$$

Where M_{AN} is the molecular mass of acrylonitrile monomer. According to eqn (7), the amount of AN-PB was found to be 790 milliequivalents grafted onto 100 g of VS. A study reported by Nagi *et al.* showed 42.3 meq of monomer grafted per 100 g of the substrate.[52]

The thermogram of AO-PB (Fig. 3(a)-D) exhibits the thermal degradation pattern by revealing its major weight loss of 25% from 115–336 °C, which is attributed to the removal of water molecules due to the hydrophilic amidoxime functional group and the onset of degradation of the polymer chains.[53] Then gradual weight loss occurred from 360–830 °C due to further decomposition of the sample. All these TGA results depict the high thermal stability of sepiolite nanoclay, which gradually decreased by the formation of polymer brushes. Onset degradation temperature of AN-PB and AO-PB starts from 570 °C and 362 °C, respectively. Decline in thermal stability of the sepiolite by the surface modification and graft polymer chains serves as a validation of the successful grafting of organic polymer brushes onto the substrate. TGA results align aptly with XRD and FTIR findings, providing robust evidence for the effective incorporation of acrylonitrile onto VS. Table 2 shows the initial decomposition temperature for 5, 10, 15 and 20% weight loss of different samples.

The comparison of the thermal stability of AN-PB and AO-PB with polyacrylonitrile and polyamidoxime homopolymer at 400 °C is shown in Table 2. Comparing the thermal stability at 400 °C, the polymer brushes synthesized through MAGP exhibit significantly higher stability than the corresponding homopolymers. This highlights the significance of grafting of these polymer chains on the thermally stable sepiolite substrate.

3.4. Crystalline structure

Fig. 3(b) displays the XRD diffractograms of PAS and its various modified polymer brushes, offering valuable insights into their structural changes. The diffractogram of PAS (Fig. 3(b)-A) typically shows a series of characteristic peaks that correspond to its crystal lattice structure. The primary reflection of PAS at $2\theta = 7.28°$ indicates the (110) plane with a *d*-spacing value of 12.2 Å.[56] Importantly, this distinctive reflection remained consistent across all the modified forms, indicating that sepiolite's fundamental structure stayed intact throughout the modification process. This diffractogram equitably matches with sepiolite JCPDS card no. 13-0595. In Fig. 3(b)-B, a slight reduction in
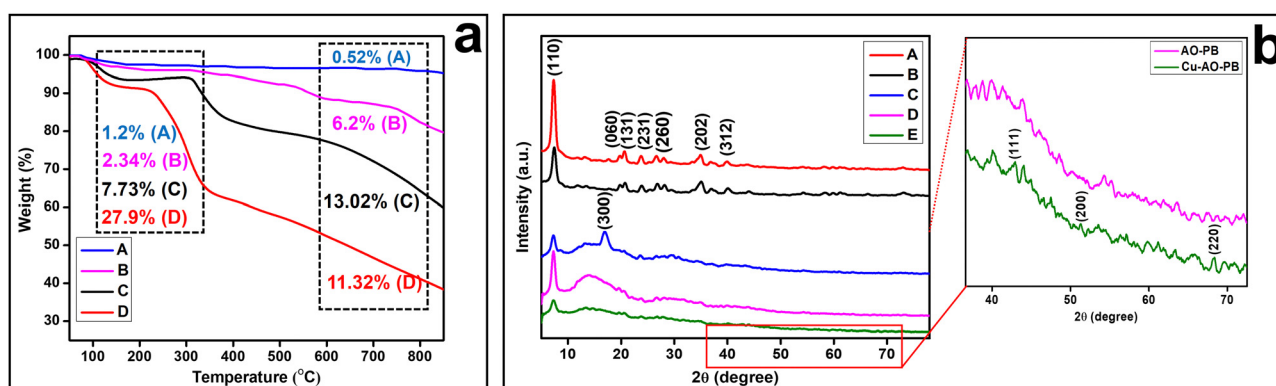

Fig. 3 (a) Comparison of the thermograms of (A) SP showing overall 3% weight loss, (B) VS showing overall 17% weight loss in 3 steps, (C) AN–PB with overall weight loss of 38% in 3 steps, (D) AO-PB with overall weight loss of 59% in 3 steps, and (b) XRD diffractograms of PAS (A), VS (B), AN–PB (C), AO-PB (D) and Cu–AO-PB (E).

Table 2 Comparison of the decomposition temperatures of SP and its various modified forms along with the comparison of the thermal stability of pure PAN HP[a] and PAO HP! with AN-PB and AO-PB at 400 °C

Sample codes	$T_{5\%}$ (°C)	$T_{10\%}$ (°C)	$T_{15\%}$ (°C)	$T_{20\%}$ (°C)
AO-PB	110.7	230	260.3	284.5
AN-PB	129.9	330	367.3	481.9
VS	365.7	566.5	760.9	838.9
SP	845	—	—	—
Samples	PAN HP*	AN-PB	PAO HP!	AO-PB
Weight loss %age till 400 °C	50	18	100	39
Ref.	54	This study	55	This study

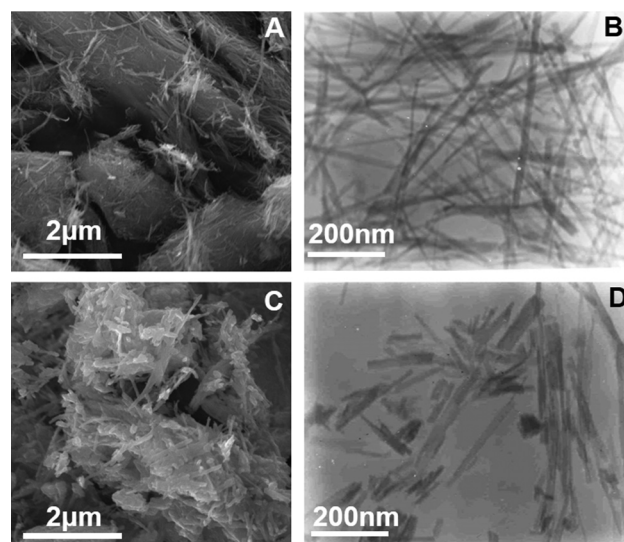[a] PAN HP = polyacrylonitrile homopolymer; PAO HP = polyamidoxime homopolymer.

peak height at $2\theta = 7.28°$ occurred, signalling the successful incorporation of VTES onto nanoclay. In Fig. 3(b)-C, a novel peak emerges at $2\theta = 16.85°$ which is credited for the (010) reflection having a d-spacing of 5.2 Å ascribed for polyacrylonitrile, evident from a noticeable hump. Additionally, a less intense peak was also observed at $2\theta = 29°$ highlighting (300) reflection. These two reflections are distinctive characteristics of AN-PB, accompanied by a decline in crystallinity of the preceding peaks, as it exhibits a semicrystalline nature and they match well with the JCPDS card no. 48-2119.[57] These observations provide fair evidence of successful grafting of AN-PB onto VS. In Fig. 3(b)-D, a new small peak appeared at $2\theta = 19.65°$ attributed to an amidoxime group,[58] and the peak at $16.85°$ disappeared corroborating successful conversion of a nitrile group to an amidoxime functionality. In Fig. 3(b)-E, three new peaks were observed (at $2\theta = 43.8°, 51°, 68.7°$) attributed to copper ions and the decrease in hump intensity also indicated the complexation of copper ions with amidoxime groups to form a chelate. All these interpretations of XRD diffractograms are aligned consistently with FT-IR and TGA outcomes.

The percentage crystallinity of the synthesized nanohybrids is calculated by using eqn (9) and displayed in Table 3. The decline in %age crystallinity from sepiolite to AO-PB serves as a validation of successful surface modification, while the increase in %age crystallinity from 47 to 50 in the case of Cu-AO-PB indicates the presence of copper ions.

$$\% \text{ Age crystallinity} = \frac{\text{Area of crystalline region}}{\text{Area of crystalline and amorphous regions}} \times 100$$

(9)

3.5. Morphological Study

The surface morphology of PS and its developed modified polymer brushes were examined using SEM coupled with EDX. The PS micrograph (Fig. 4(A)) shows the needle like morphology of the nanoclay. The individual fibers appear long and thin, with high aspect ratio, and they are randomly

Table 3 Percentage crystallinity of sepiolite and its various modified forms

Samples	PAS	VS	AN-PB	AO-PB	Cu-AO-PB
%age Crystallinity	71	68	54	47	50

Fig. 4 SEM and TEM images of pristine sepiolite and its vinyl modified form: SEM of PS (A), VS (C), TEM of PS (B) and VS (D).

oriented and exhibit some degree of agglomeration. Following the vinyl modification, a noticeable rough surface texture transformation occurred (Fig. 4(C)).

The TEM micrograph of PS (Fig. 4(B)), shows the structure of the individual fibers, including the presence of channels and pores within the crystal lattice. By comparing the TEM micrographs of PS and VS (Fig. 4(B) and (D)), it is evident that the diameter of the nanofibers is increased (from around 8–12 nm to 10–25 nm) whereas the length of the nanofibers is decreased (from 20 nm–1.5 μm to 5–600 nm).[23,59] The altered morphology of the nanofibers in VS, with the emergence of smaller fibers having uneven surfaces, not only provides evidence of surface functionalization by VTES but also suggests that shortened fibers of VS are helpful to enter into micelles generated by surfactant polysorbate 80.[60] This indicates that VTES treatment has led to a higher degree of surface exposure, which is consistent with the process of surface modification.

These variations resulting from the modification process, such as the presence of amorphous regions, the distribution of the modifying agent within the structure, or changes in the crystalline orientation of the fibers, substantiate the surface modification by VTES, which is also supported by FTIR, XRD and TGA analyses.[23]
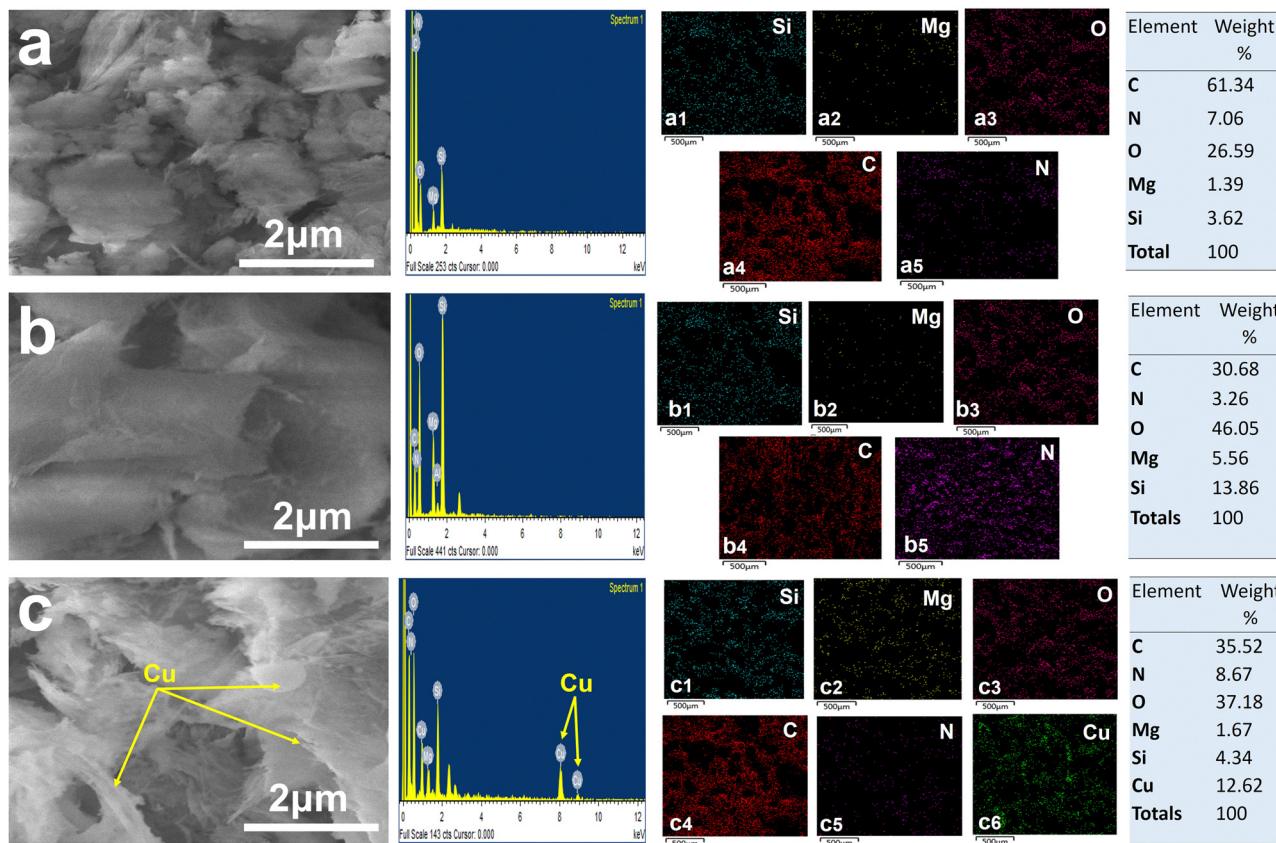
Fig. 5 (a) SEM and EDX of AN-PB with a1 to a5 show the corresponding Si, O, Mg, C and N mapping, (b) SEM and EDX of AO-PB with b1 to b5 shows the corresponding Si, O, Mg, C and N mapping, (c) SEM and EDX of Cu-AO-PB with c1 to c6 showing the corresponding Si, O, Mg, C, N and Cu mapping.

SEM micrograph, elemental analysis and mapping of AN-PB are shown in Fig. 5(a). The morphology of AN-PB determines that VS fibers are enfolded by polyacrylonitrile chains. EDX maps showed the presence of Si, Mg, O, C and N atoms, which are evenly distributed throughout the sample, demonstrating the grafting of polyacrylonitrile onto VS[61] and the weight % of constituent elements is also presented in Fig. 5 (from a1 to a5). Fig. 5(b) illustrates the distinct morphology and smooth surface of AO-PB. EDX maps and elemental analysis of nitrogen and oxygen atoms in AO-PB are showing greater concentration than the same maps of AN-PB, validating the modification of polyacrylonitrile to a polyamidoxime group.[62] The SEM micrograph of copper loaded AO-PB after chelation is shown in Fig. 5(c). The granular texture of Cu-AO-PB in the micrograph and the existence of copper in the sample shown by EDX maps demonstrates the uniformity in copper distribution, which signifies the efficient chelation, thus confirming the presence of active sites within the polymer brush with even distribution. The distribution of weight% of constituent elements is presented in Fig. 5 (from c1 to c6).

The SEM and EDX results are consistent with XRD, FTIR and TGA analyses, reinforcing the conclusion that the structural integrity of clay remained intact and functionalization primarily targets the surface. All these morphological revelations provide an insight into the structural transformations and functionalization procedures undertaken by these materials.

3.6. Catalytic reduction of 4-NP

There are numerous reactions that require an efficient catalytic system as it provides a means of reducing the activation energy and increasing the reaction rate. Heterogeneous catalysis is extensively favored due to its number of benefits over homogenous catalysis including stability, recyclable nature, and facile separation from the reaction medium, ultimately resulting in low operating costs.

4-NP conversion to 4-AP was selected as a model reduction reaction to test the efficacy of Cu-AO-PB as a catalyst. The absorption band of 4-NP in neutral and acidic solution is at 317 nm,[63] as shown in Fig. 6(A). However, when $NaBH_4$ was added, the deprotonation of the hydroxyl group of 4-NP occurred resulting in a bathochromic shift to 400 nm due to the formation of nitrophenolate ions having dark yellow coloration. As a blank experiment, AO-PB was introduced into nitrophenolate ion solution to assess its catalytic ability but an electronic band at about 295 nm assigned to 4-AP was not observed, demonstrating that 4-NP did not reduce without metal loaded polymer brushes. After the addition of Cu-AO-PB catalyst, the electronic absorption peak at 400 nm gradually reduced in intensity and a new peak originated at 295 nm which was attributed to 4-AP. Within 360 seconds, the electronic band at 400 nm completely disappeared indicating the completion of 4-NP reduction to 4-AP (Fig. 6(B)).[64] A peak is also present at
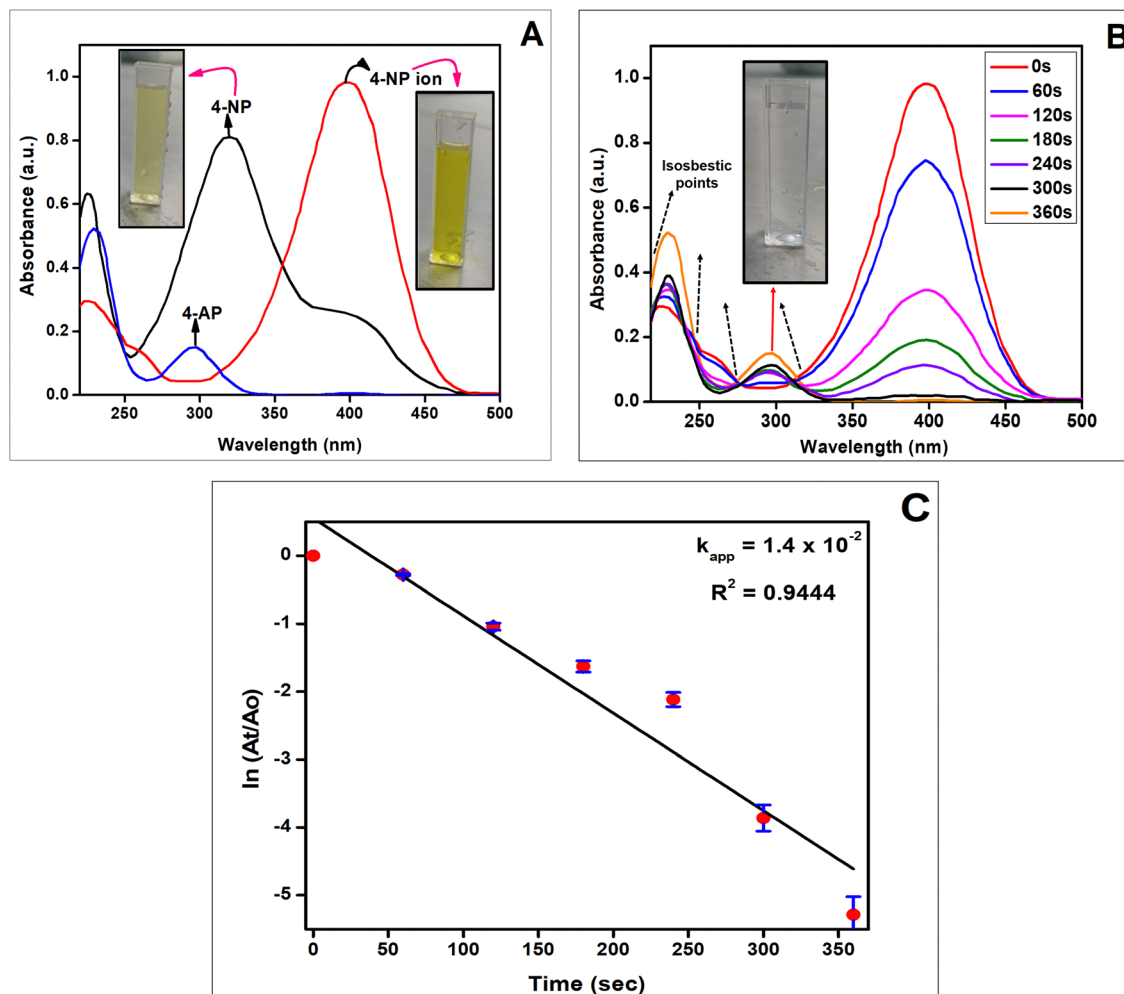
Fig. 6 (A) Time dependent UV-visible study of 4-NP to 4-AP by the Cu–AO-PB catalyst, indicating light yellow colored solution of 4-NP and its adsorption peak is present at 317 nm; after the addition of NaBH$_4$, the absorption peak shifts at 400 nm having dark yellow colored solution due to 4-nitrophenolate ions. Subsequent addition of catalyst leads to complete disappearance of this peak within 360 seconds with the origination of a new peak at 295 nm indicating 4-AP, (B) kinetic study of reduction reaction by Cu–AO-PB, (C) pseudo-first order plot of time verses ln (A_t/A_o) and rate constant computed by the slope of the line ($k_{app} = 1.4 \times 10^{-2}$).

approximately 224 nm in the UV-Visible spectra of both 4-NP and 4-AP (Fig. 6(A) and (B)). This absorption peak is characteristic of electronic transition associated with the aromatic ring.[65] The presence of four isosbestic points in Fig. 6(B) demonstrates the absence of any side products.[66] In Fig. 6(C), pseudo-first order plot is displayed between ln A_t/A_o and time and the apparent rate constant (k_{app}) determined by the slope of the line is 0.0143 s^{-1}.

The comparison of the rate constant of Cu–AO-PB with different reported catalysts for 4-NP reduction is presented in Table 5. It is worth stating that Cu–AO-PB is a much better catalyst accredited to special characteristics of the sepiolite support containing metal-loaded polymer chains. The polymer brushes carrying copper metal ions expedite the reaction by engaging π–π interactions with 4-NP, which facilitates the electron transfer from BH$_4^-$ to the sp^2-hybridized NO$_2$ group of 4-NP.

3.6.1. The Langmuir–Hinshelwood mechanism of 4-NP Reduction by Cu–AO-PB. The 4-NP reduction is a complex
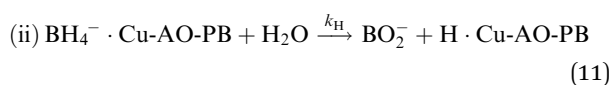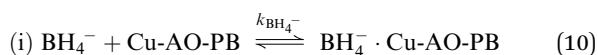
process involving adsorption and interfacial electron transfer on the surface of the Cu-loaded polyamidoxime brush. Borohydrides exhibit significant capability of hydrogen generation making the study of their reaction with metallic surfaces a crucial focus of recent research. The Langmuir–Hinshelwood model has been employed to elucidate the reaction mechanism for 4-NP reduction occurring on the Cu–AO-PB catalyst's surface shown in Scheme 2. The reaction unfolds in two stages, the first stage is composed of two steps, (i) the equilibrized adsorption of BH$_4^-$ ions with the Cu–AO-PB surface (eqn (10)) and (ii) the formation of active hydrogen species (AHS) on the Cu–AO-PB surface (eqn (11)).[67] The second stage comprised three steps, (i) the equilibrized adsorption of 4-nitrophenolate ions on the polymer brush (eqn (12)), (ii) 4-NP reduction occurred at the surface of the catalyst adsorbed by BH$_4^-$ ions and 4-NP by 6 active hydrogen species (AHS) to form 4-AP through the formation of the 4-hydroxylaminophenol intermediate (eqn (13)), and (iii) the elimination of two H$_2$O molecules from the nitro group, and lastly the removal of the 4-AP from the surface of the
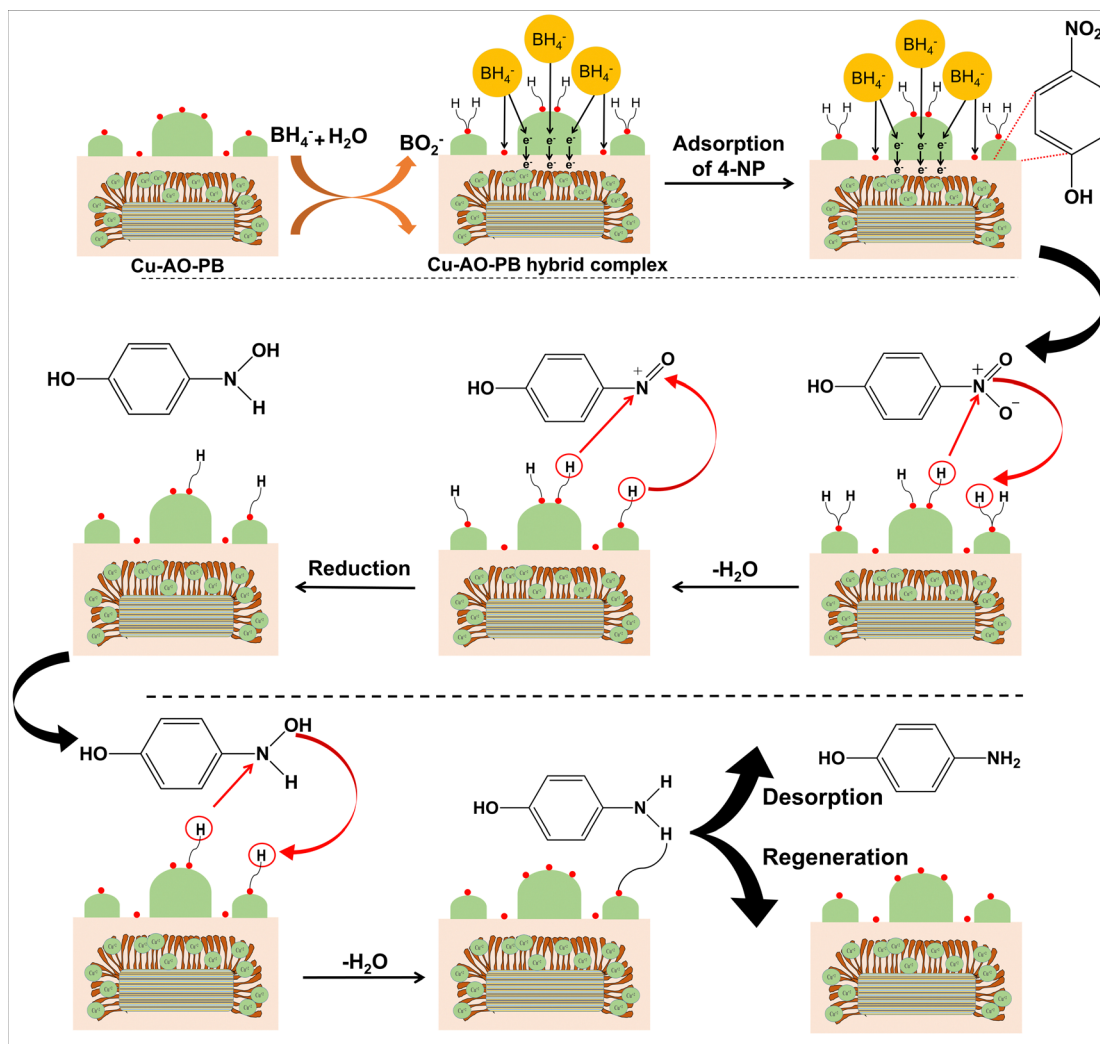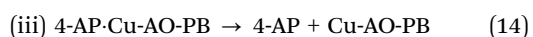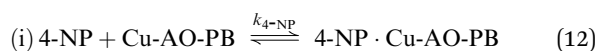
Scheme 2 Possible illustration of the mechanism for the conversion of 4-NP into 4-AP catalyzed by Cu-AO-PB according to the Langmuir–Hinshelwood model.

Cu-AO-PB polymer brush leaving the catalyst ready for the next catalytic cycle (eqn (14)).

Stage 1:

$$\text{(i) BH}_4^- + \text{Cu-AO-PB} \underset{}{\overset{k_{\text{BH}_4^-}}{\rightleftharpoons}} \text{BH}_4^- \cdot \text{Cu-AO-PB} \quad (10)$$

$$\text{(ii) BH}_4^- \cdot \text{Cu-AO-PB} + \text{H}_2\text{O} \xrightarrow{k_{\text{H}}} \text{BO}_2^- + \text{H} \cdot \text{Cu-AO-PB} \quad (11)$$

Stage 2:

$$\text{(i) 4-NP} + \text{Cu-AO-PB} \underset{}{\overset{k_{\text{4-NP}}}{\rightleftharpoons}} \text{4-NP} \cdot \text{Cu-AO-PB} \quad (12)$$

$$\text{(ii) 4-NP} \cdot \text{Cu-AO-PB} + 6\text{H(AHS)} \xrightarrow{k} \text{4-AP} \cdot \text{Cu-AO-PB} + 2\text{H}_2\text{O} \quad (13)$$

$$\text{(iii) 4-AP} \cdot \text{Cu-AO-PB} \rightarrow \text{4-AP} + \text{Cu-AO-PB} \quad (14)$$

The adsorption and desorption of BH_4^- and 4-NP (eqn (9) and (11)) occur rapidly on the catalyst's surface, having no impact on the kinetic equation. Stage 2, reaction (ii) is considered the rate determining step where 4-NP is converted to 4-AP by AHS (eqn (13)).

3.6.2. Optimization of different parameters for the catalytic reaction. The optimization of various key parameters in the 4-NP reduction reaction was undertaken to ameliorate the efficiency of the catalytic system. These parameters include the catalyst dosage, concentrations of 4-NP and NaBH$_4$, and the reaction temperature.

To assess the catalysts' impact on 4-NP reduction, the catalyst dose was altered ranging from 20 mg to 100 mg while keeping other parameters constant and it was found that the k_{app} values increased with catalyst dose, as shown in Fig. 7(A). This outcome is attributed to the surface transfer nature of the 4-NP reduction reaction, where a higher catalyst dose introduces an increased surface–volume ratio and an abundance of active sites for the BH_4^- ion and 4-NP.[68] Moreover, the effect of 4-NP concentration was explored (ranging from 2 mM to 10 mM) on its reduction, keeping the concentration of NaBH$_4$ at 10 mM and catalyst amount at 0.1 g. Fig. 7(B) displays the
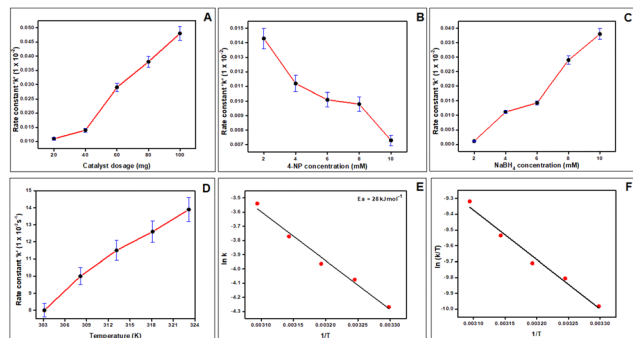
Fig. 7 Detailed UV study of various reaction parameters, (A) effect of catalyst dose on rate constant, (B) effect of 4-NP conc. on rate constant, (C) effect of NaBH$_4$ conc. on rate constant, (D) effect of temperature on rate constant, (E) Arrhenius plot, here $1/T$ is plotted vs. $\ln k$ and activation energy is calculated from slope of the line, (F) plot of $1/T$ versus $\ln (k/T)$ to calculate thermodynamic parameters: ΔH, ΔS and ΔG.

$\ln(C/C_0)$ dependency on time, revealing that the k value decreased with rising 4-NP concentration. Lower concentrations resulted in more efficient conversion of 4-NP, as fewer 4-NP molecules competed for active sites with NaBH$_4$. This led to more efficient conversion of 4-NP, whereas sluggish electron transfer and a lowered reduction rate were observed at higher 4-NP concentrations.[69] Similarly, the influence of NaBH$_4$ concentration was investigated (ranging from 2 mM to 10 mM) on 4-NP reduction while keeping other parameters constant. Rate constants were determined from the slope of the line, showing an increase in k with higher NaBH$_4$ concentration (Fig. 7(C)). Lower concentration of NaBH$_4$ provides fewer BH$_4^-$ ions and in turn fewer electrons are available for 4-NP, resulting in a slower electron transfer process and a lower rate constant. Conversely, higher concentration of NaBH$_4$ supplied more BH$_4^-$, facilitating quicker reduction through swift electron transfer.[70] Furthermore, the catalytic performance of the Cu-AO-PB polymer brush for 4-NP reduction was studied at five temperature variations of 303 K, 308 K, 313 K, 318 K, and 323 K, while maintaining the amounts of catalyst (0.1 g), 4-NP (2 mM), and NaBH$_4$ (10 mM) constant as displayed in Fig. 7(D). It was evident that higher temperatures were associated with an increase in k, in line with the collision theory. In chemical reactions, elevated temperatures promote increased kinetic energy among molecules resulting in more frequent collisions, thus accelerating the reaction rate.[71]

3.6.3. Thermodynamic study. The thermodynamic parameters for catalytic reduction by Cu-AO-PB were analyzed at five different temperatures extending from 303 K to 323 K. The activation energy was calculated by the Arrhenius equation.

$$\ln k = \ln A - (E_a/RT) \quad (15)$$

E_a denotes the activation energy, A represents the Arrhenius constant, R is the universal gas constant, and k symbolizes the rate constant at temperature T. Activation energy is calculated from the linear plot of $\ln k$ vs. $1/T$ (Fig. 7(E)) and it came out to be 28 kJmol^{-1}. The obtained low E_a value is attributed to high catalytic activity of the Cu-AO-PB polymer brush. Typically, for

Table 4 Temperature dependency of the rate of 4-NP reduction with the Cu-AO-PB catalyst and different thermodynamic parameters calculated from temperature study

Temperature (K)	k (s^{-1})	ΔS (J mol^{-1} k^{-1})	ΔH (kJ mol^{-1})	ΔG (kJ mol^{-1})
303	0.014	−214.036	−25.99	64.85
308	0.017	—	—	65.92
313	0.019	—	—	66.99
318	0.023	—	—	68.12
323	0.029	—	—	69.13

surface-catalyzed reactions, the activation energy falls within 8.37–41.84 KJ mol^{-1}.[72] This suggests that the reduction of 4-NP by Cu-AO-PB polymer brushes occurs through surface catalysis. Moreover, this inference is reinforced by the observed order of the reaction. Table 5 presents the comparison of the E_a value of Cu-AO-PB with different reported catalysts.

Additionally, enthalpy change (ΔH) and entropy change (ΔS) were computed by means of the Eyring equation.[73]

$$\ln\left(\frac{k}{T}\right) = \ln\left(\frac{k_B}{h}\right) + \frac{\Delta S}{R} - \frac{\Delta H}{R}\left(\frac{1}{T}\right) \quad (16)$$

Here, k_B denotes the Boltzmann constant, h represents Planck's constant, and the enthalpy and entropy changes are designated by ΔH and ΔS, respectively.

These parameters were determined by analyzing the slope of $\ln k/T$ against $1/T$ and the results are presented in Table 4. ΔG was calculated for 303 K to 323 K by using the Gibbs–Helmholtz equation (eqn (17)) and the results are also presented in Table 4. ΔG designates the barrier for 4-nitrophenol to cross to reach the activated state. Gibbs free energy was enlarged from 64.85 kJ mol^{-1} at 303 K to 69.13 kJ mol^{-1} at 323 K which signifies the requirement of energy for this reaction.

$$\Delta G = \Delta H - T\Delta S \quad (17)$$

3.6.4. Turnover frequency (TOF). TOF value can provide valuable insight into catalyst stability and activity. It indicates the numerals of reactant molecules that are transformed into products by 1 g of catalytic material within the given time frame. TOF was calculated by using eqn (18) where $n_{4\text{-NP}}$ and $n_{\text{Cu-AO-PB}}$ represent the number of moles of 4-NP and Cu-AO-PB, respectively, t_{red} signifies the time for 4-NP reduction in hours, and the factor 0.98 signifies a completion percentage of 98%.[74]

$$\text{TOF} = \frac{n_{4\text{-NP}}}{n_{\text{Cu-AO-PB}} \times t_{\text{red}}} \times 0.98 \quad (18)$$

The TOF value is estimated to be 1.65×10^{10} molecules g^{-1} sec^{-1} at ambient temperature, which emphasized that 1.65×10^{10} molecules of 4-NP are reduced into 4-AP by 1 g of Cu-AO-PB per second. As is known from the literature, a high TOF indicates rapid catalytic turnover, which is desirable for various chemical processes.[75] It also implies that this catalyst is potentially suitable for promoting high reaction rates. The comparison of this TOF value by Cu-AO-PB with different reported catalysts is presented in Table 5.

Table 5 Comparison of Ea and TOF of Cu-AO-PB with different copper-based reported catalysts for 4-NP reduction

Catalyst	k (s^{-1})	Ref.	Catalyst	E_a (kJ mol^{-1})	Ref.	Catalyst	TOF (s^{-1})	Ref.
Cu cubes (9.5 nm)	0.0101	76	Cu-NPANI-ZrSiO$_4$	85.06	77	Cu cubes	4.8×10^5	78
Cu NPs (12.5 mg)	0.0016	79	CuCo$_2$O$_4$/BiVO$_4$	29.88	80	SiNWAS-Cu	7.9×10^5	81
Cu–Ag bimetallic NPs	0.0073	82	Nitrogen doped carbon-encapsulated copper composite	55.6	83	Cu/BNO	26.4	84
Cu nanoplates	0.0095	85	Cu–COF	31	86	Cu@ZIF-67	90	87
Porous Cu-microsphere	0.0043	88	Copper cages	34.8	89	Cu,Co@PC	3.12×10^2	87
Cu nanowires	0.0042	90	27.8 nm Cu NPs	74.0	91	Cu hexa cyano ferrate nanocrystal	2.2×10^3	92
Cu–COF	0.0047	82	18.0 nm Cu polyhedrons	47.6	93	Mn$_3$O$_4$/PdCu@NC	2.6×10^6	94
Cu-AO-PB	0.0143	This study	Cu-AO-PB	28	This Study	Cu-AO-PB	1.65×10^{10}	This study
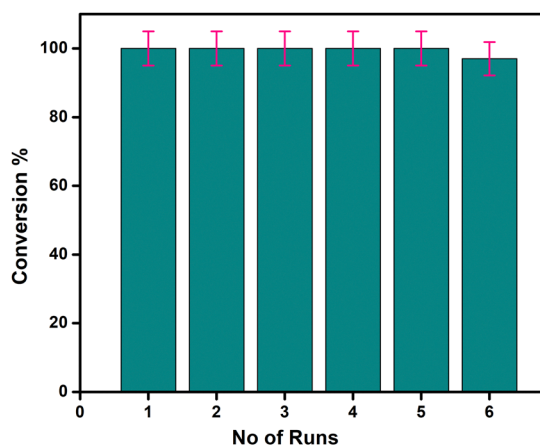
Fig. 8 Recyclability of the Cu-AO-PB polymer brush for the conversion of 4-NP to 4-AP.

3.6.5. Recyclability study. The recovery and reuse of heterogeneous catalysts is an imperative factor while evaluating their performance. The reaction was repeated 6 times using the same conditions (0.20 mM 4-NP, 10 mM NaBH$_4$, 0.1 g Cu-AO-PB at room temperature), the catalyst was separated *via* filtration and reused successively 5 times with 100% efficiency. At the 6th cycle, the conversion efficiency was decreased to 96% as depicted in Fig. 8.

4. Conclusions

This research study presents significant advancements in heterogeneous catalysis through the innovative application of MAGP for synthesizing Cu-AO-PB. Microwave irradiation accelerated the polymerization rate, reducing the synthesis time by approximately 20-fold compared to conventional methods. Optimization of the grafting parameters (time, power, monomer, initiator, substrate and surfactant concentration) of acrylonitrile onto VS resulted in the grafting percentage of 449% with 89% grafting efficiency. Through the comprehensive analysis of various characterization techniques, the prepared nanohybrid polymer brushes have demonstrated well-defined morphology and chemical composition.

The close correspondence between the observed morphological changes in the SEM and TEM images, structural composition by FTIR spectra and the alterations in the crystalline structure detected by XRD, indicate successful grafting and surface modification. TGA thermograms of all synthesized nanohybrids exhibit good thermal stability. In the case of sepiolite, only 3% weight loss occurs until 800 °C, while VS shows overall 17%, AN-PB shows 38% and only 59% weight loss occurs for AO-PB until this temperature. So, TGA depicts high thermal stability of the substrate, which gradually decreased by the grafting of polymeric chains onto the substrate. The grafted polymer brushes exhibited significantly higher thermal stability at 400 °C compared to the corresponding homopolymers.

The catalytic performance of Cu-AO-PB was systematically evaluated using UV-VIS spectroscopy and reaction kinetic studies, establishing a marked improvement in reaction time and conversion efficiency in comparison with reported work. Thermodynamic parameters, like ΔS (−214.036 Jmol^{-1}), ΔH (−25.99 kJmol^{-1}), ΔG (64.85 kJmol^{-1}) and E_a were computed from the Eyring and Arrhenius equations. A lower activation energy value of 28 kJ mol^{-1} associated with a higher rate constant (0.0143 s^{-1}), signifies that the reaction proceeds at a faster rate, especially at elevated temperatures, due to the reduced energy barrier. The TOF value of this nanohybrid material for 4-NP reduction was calculated to be 1.65×10^{10} molecules g^{-1} s^{-1}. These findings highlight the potential of MAGP in synthesizing highly efficient functional polymer brushes with enhanced thermal stability and catalytic performance. With the optimized conditions for maximum conversion and impressive stability over multiple cycles, this system offers a sustainable solution for heterogeneous catalysis setups, paving the way for greener and more efficient chemical processes.

Author contributions

S. T.: conceptualization, writing – original draft, writing – review & editing, methodology, investigation, formal analysis, visualization, supervision, resources, project administration, S. R.: investigation, writing – original draft, M. E.: visualization, project management, S. R.: resources, validation, H. R.: resources,

writing – review & editing, T. Y.: resources, writing – review & editing.

Data availability

Data will be made available on request.

Conflicts of interest

The authors declare that they have no known competing financial interests or personal relationships that could have appeared to influence the work reported in this paper.

Acknowledgements

References

1 O. Azzaroni, Polymer brushes here, there, and everywhere: Recent advances in their practical applications and emerging opportunities in multiple research fields, *J. Polym. Sci., Part A: Polym. Chem.*, 2012, **50**, 3225–3258, DOI: **10.1002/pola.26119**.

2 S. T. Milner, Polymer Brushes, *Science*, 1979, **251**, 905–914, DOI: **10.1126/science.251.4996.905**.

3 E. Beyou and E. Bourgeat-Lami, Organic–inorganic hybrid functional materials by nitroxide-mediated polymerization, *Prog. Polym. Sci.*, 2021, **121**, 101434, DOI: **10.1016/j.progpolymsci.2021.101434**.

4 C. Feng and X. Huang, Polymer Brushes: Efficient Synthesis and Applications, *Acc. Chem. Res.*, 2018, **51**, 2314–2323, DOI: **10.1021/acs.accounts.8b00307**.

5 H. Moustafa, A. M. Youssef, N. A. Darwish and A. I. Abou-Kandil, Eco-friendly polymer composites for green packaging: Future vision and challenges, *Composites, Part B*, 2019, **172**, 16–25, DOI: **10.1016/j.compositesb.2019.05.048**.

6 K. Kempe, C. R. Becer and U. S. Schubert, Microwave-Assisted Polymerizations: Recent Status and Future Perspectives, *Macromolecules*, 2011, **44**, 5825–5842, DOI: **10.1021/ma2004794**.

7 M. B. Gawande, S. N. Shelke, R. Zboril and R. S. Varma, Microwave-Assisted Chemistry: Synthetic Applications for Rapid Assembly of Nanomaterials and Organics, *Acc. Chem. Res.*, 2014, **47**, 1338–1348, DOI: **10.1021/ar400309b**.

8 L. Zong, S. Zhou, N. Sgriccia, M. C. Hawley and A. Kempel, review of microwave-assist polymer chemistry (MAPC, *J. Microw. Power Electromagn. Energy*, 2003, **38**, 49–74, DOI: **10.1080/08327823.2003.11688487**.

9 R. R. Mishra and A. K. Sharma, Microwave–material interaction phenomena: Heating mechanisms, challenges and opportunities in material processing, *Composites, Part A*, 2016, **81**, 78–97, DOI: **10.1016/j.compositesa.2015.10.035**.

10 D. Zheng, K. Liu, Z. Zhang, Q. Fu, M. Bian, X. Han and S. Song, Essential features of weak current for excellent enhancement of NOx reduction over monoatomic V-based catalyst, *Nat. Commun.*, 2024, **15**, 6688, DOI: **10.1038/s41467-024-51034-0**.

11 S. V. Orski, K. H. Fries, S. K. Sontag and J. Locklin, Fabrication of nanostructures using polymer brushes, *J. Mater. Chem.*, 2011, **21**, 14135–14149, DOI: **10.1039/C1JM11039J**.

12 Z. Ahmad, *et al.*, A Membrane-Supported Bifunctional Poly(amidoxime-ethyleneimine) Network for Enhanced Uranium Extraction from Seawater and Wastewater, *J. Hazard. Mater.*, 2022, **425**, 127995, DOI: **10.1016/j.jhazmat.2021.127995**.

13 B. K. Singh, M. Asim, Z. Salkenova, D. Pak and W. Um, Engineered Sorbents for Selective Uranium Sequestration from Seawater, *ACS EST Water*, 2024, **4**, 325–345, DOI: **10.1021/acsestwater.3c00516**.

14 F. Yang and A. Wang, Recent researches on antimicrobial nanocomposite and hybrid materials based on sepiolite and palygorskite, *Appl. Clay Sci.*, 2022, **219**, 106454, DOI: **10.1016/j.clay.2022.106454**.

15 Z. Iqbal Khan, U. Habib, Z. Binti Mohamad, A. Razak Bin Rahmat and N. Amira Sahirah Binti Abdullah, Mechanical and thermal properties of sepiolite strengthened thermoplastic polymer nanocomposites: A comprehensive review, *Alexandria Eng J.*, 2022, **61**, 975–990, DOI: **10.1016/j.aej.2021.06.015**.

16 H. N. Abdelhamid, High performance and ultrafast reduction of 4-nitrophenol using metal-organic frameworks, *J. Environ. Chem. Eng.*, 2021, **9**, 104404, DOI: **10.1016/j.jece.2020.104404**.

17 A. Serrà, R. Artal, M. Pozo, J. Garcia-Amorós and E. Gómez, Simple Environmentally-Friendly Reduction of 4-Nitrophenol, *Catalysis*, 2020, **10**, 458, DOI: **10.3390/catal10040458**.

18 A. Hojjati-Najafabadi, M. Mansoorianfar, T. Liang, K. Shahin and H. Karimi-Maleh, A review on magnetic sensors for monitoring of hazardous pollutants in water resources, *Sci. Total Environ.*, 2022, **824**, 153844, DOI: **10.1016/j.scitotenv.2022.153844**.

19 M. Bilal, A. R. Bagheri, P. Bhatt and S. Chen, Environmental occurrence, toxicity concerns, and remediation of recalcitrant nitroaromatic compounds, *J. Environ. Manage.*, 2021, **291**, 112685, DOI: **10.1016/j.jenvman.2021.112685**.

20 Z. Wang, *et al.*, Sulfurized Graphene as Efficient Metal-Free Catalysts for Reduction of 4-Nitrophenol to 4-Aminophenol, *Ind. Eng. Chem. Res.*, 2017, **56**, 13610–13617, DOI: **10.1021/acs.iecr.7b03217**.

21 A. Kumar, Y. Kuang, Z. Liang and X. Sun, Microwave chemistry, recent advancements, and eco-friendly microwave-assisted synthesis of nanoarchitectures and their applications: a review, *Mater. Today Nano*, 2020, **11**, 100076, DOI: **10.1016/j.mtnano.2020.100076**.

22 S. Taimur, M. I. Hassan and T. Yasin, Removal of copper using novel amidoxime based chelating nanohybrid adsorbent, *Eur. Polym. J.*, 2017, **95**, 93–104, DOI: **10.1016/j.eurpolymj.2017.08.004**.

23 S. Taimur and T. Yasin, Influence of the synthesis parameters on the properties of amidoxime grafted sepiolite

nanocomposites, *Appl. Surf. Sci.*, 2017, **422**, 239–246, DOI: **10.1016/j.apsusc.2017.05.263**.

24 A. Mazloom Jalali, F. Afshar Taromi, M. Atai and L. Solhi, Effect of reaction conditions on silanisation of sepiolite nanoparticles, *J. Exp. Nanosci.*, 2016, **11**, 1171–1183, DOI: **10.1080/17458080.2016.1200147**.

25 Z. Hou, D. Zhou, Q. Chen and Z. Xin, Effect of Different Silane Coupling Agents In-Situ Modified Sepiolite on the Structure and Properties of Natural Rubber Composites Prepared by Latex Compounding Method, *Polymers*, 2023, **15**, 1620, DOI: **10.3390/polym15071620**.

26 C. Sanchez, P. Belleville, M. Popall and L. Nicole, Applications of advanced hybrid organic–inorganic nanomaterials: from laboratory to market, *Chem. Soc. Rev.*, 2001, **40**, 696–753, DOI: **10.1039/C0CS00136H**.

27 N. Mehio, A. S. Ivanov, N. J. Williams, R. T. Mayes, V. S. Bryantsev, R. D. Hancock and S. Dai, Quantifying the binding strength of salicylaldoxime–uranyl complexes relative to competing salicylaldoxime–transition metal ion complexes in aqueous solution: a combined experimental and computational study, *Dalton Trans.*, 2016, **45**, 9051–9064, DOI: **10.1039/C6DT00116E**.

28 C. V. Chaudhari, K. A. Dubey, N. K. Goel, Y. K. Bhardwaj and L. Varshney, Correlation between surface energy and uptake behavior of radiation-grafted methacrylic acid-g-LDPE, *Polym. Bull.*, 2012, **69**, 779–793, DOI: **10.1007/s00289-012-0767-1**.

29 K. M. Mostafa and A. A. El-Sanabary, Green and efficient tool for grafting acrylonitrile onto starch nanoparticles using microwave irradiation, *J. Polym. Res.*, 2020, **27**, 1–10, DOI: **10.1016/j.progpolymsci.2017.11.002**.

30 C. O. Kappe, Controlled Microwave Heating in Modern Organic Synthesis, *Angew. Chem., Int. Ed.*, 2004, **43**, 6250–6284, DOI: **10.1002/anie.200400655**.

31 K. C. Gupta and S. Sahoo, Graft Copolymerization of Acrylonitrile and Ethyl Methacrylate Comonomers on Cellulose Using Ceric Ions, *Biomacromolecules*, 2001, **2**, 239–247, DOI: **10.1021/bm000102h**.

32 N. Ballard and J. M. Asua, Radical polymerization of acrylic monomers: An overview, *Prog. Polym. Sci.*, 2018, **79**, 40–60, DOI: **10.1016/j.progpolymsci.2017.11.002**.

33 B. Yamada and P. B. Zetterlund, General chemistry of radical polymerization, *Handbook of Radical Polymerization*, 2002, pp. 117–186, DOI: **10.1002/0471220450**.

34 W. Mehnert and K. Mäder, Solid lipid nanoparticles: production, characterization and applications, *Adv. Drug Delivery Rev.*, 2012, **64**, 83–101, DOI: **10.1016/j.addr.2012.09.021**.

35 C. Sharma, M. A. Desai and S. R. Patel, Effect of surfactants and polymers on morphology and particle size of telmisartan in ultrasound-assisted anti-solvent crystallization, *Chem. Pap.*, 2019, **73**, 1685–1694, DOI: **10.1007/s11696-019-00720-1**.

36 C. Ebner, T. Bodner, F. Stelzer and F. Wiesbrock, One Decade of Microwave-Assisted Polymerizations: Quo vadis, *Macromol. Rapid Commun.*, 2011, **32**, 254–288, DOI: **10.1002/marc.201000539**.

37 A. Halmagyi, E. Surducan and V. Surducan, The effect of low- and high-power microwave irradiation on *in vitro* grown Sequoia plants and their recovery after cryostorage, *J. Biol. Phys.*, 2017, **43**, 367–379.

38 H. A. Yousef, B. M. Alotaibi, A. Atta, E. Abdeltwabb and M. M. A. Hamidc, Fabrication, characterization and effects of CuO nanoparticles on the optical behavior of polypyrrole polymeric films, *Digest J. Nanomater. Biostruct.*, 2024, **19**, DOI: **10.15251/DJNB.2024.191.151**.

39 V. Singh and D. N. Tripathi, Microwave promoted grafting of acrylonitrile onto Cassia siamea seed gum, *J. Appl. Polym. Sci.*, 2006, **101**, 2384–2390, DOI: **10.1002/app.23878**.

40 A. Bashir, R. Malviya and K. Sharma, Microwave Assisted Grafting of Natural Polysaccharides, J. Chronother, *Drug Delivery*, 2015, **6**, 79–92.

41 V. Singh, P. L. Kumari, A. Tiwari and A. K. Sharma, Alumina supported synthesis of Cassia marginata gum-g-poly(acrylonitrile) under microwave irradiation, *Polym. Adv. Technol.*, 2007, **18**, 379–385, DOI: **10.1002/pat.899**.

42 D. Kumar, J. Pandey and P. Kumar, Microwave assisted synthesis of binary grafted psyllium and its utility in anti-cancer formulation, *Carbohydr. Polym.*, 2018, **179**, 408–414, DOI: **10.1016/j.carbpol.2017.09.093**.

43 V. Singh, A. Tiwari, S. Pandey and S. K. Singh, Peroxydisulfate initiated synthesis of potato starch-*graft*-poly(acrylonitrile) under microwave irradiation, *eXPRESS Polym. Lett.*, 2007, **1**, 51–58, DOI: **10.3144/expresspolymlett.2007.10**.

44 A. I. Al-Ghonamy and M. A. Barakat, Study of the Effect of Grafted Antioxidant on the Acrylonitrile-Butadiene Copolymer Properties, *Int. J. Polym. Sci.*, 2010, **2010**, 1–7, DOI: **10.1155/2010/359015**.

45 A. Walczyk, *et al.*, New insight into the phase transformation of sepiolite upon alkali activation: Impact on composition, structure, texture, and catalytic/sorptive properties, *Appl. Clay Sci.*, 2020, **195**, 105740, DOI: **10.1016/j.clay.2020.105740**.

46 V. Pratap Singh, G. S. Kapur, S. Shashikant and V. Choudhary, High-density polyethylene/needle-like sepiolite clay nanocomposites: effect of functionalized polymers on the dispersion of nanofiller, melt extensional and mechanical properties, *RSC Adv.*, 2016, **6**, 59762–59774, DOI: **10.1039/C6RA08124J**.

47 F. Altaf, R. Batool, M. A. Ahmad, R. Raza, M. A. Khan and G. Abbas, Novel vinyl-modified sepiolite-based polymer nanocomposites: synthesis and characterization, *Iran. Polym. J.*, 2018, **27**, 413–422, DOI: **10.1007/s13726-018-0619-4**.

48 R. Ganfoud, L. Puchot, T. Fouquet and P. Verge, H-bonding supramolecular interactions driving the dispersion of kaolin into benzoxazine: A tool for the reinforcement of polybenzoxazines thermal and thermo-mechanical properties, *Compos. Sci. Technol.*, 2015, **110**, 1–7, DOI: **10.1016/j.compscitech.2015.01.014**.

49 I. Karacan and G. Erdogan, The influence of thermal stabilization stage on the molecular structure of polyacrylonitrile fibers prior to the carbonization stage, *Fibers Polym.*, 2012, **13**, 295–302, DOI: **10.1007/s12221-012-0295-5**.

50 S. Zhuang and J. Wang, Poly amidoxime functionalized carbon nanotube as an efficient adsorbent for removal of

uranium from aqueous solution, *J. Mol. Liq.*, 2020, **319**, 114288, DOI: **10.1016/j.molliq.2020.114288**.

51 G. Tartaglione, D. Tabuani and G. Camino, Thermal and morphological characterisation of organically modified sepiolite, *Microporous Mesoporous Mater.*, 2008, **107**, 161–168, DOI: **10.1016/j.micromeso.2007.04.020**.

52 N. Greesh, S. Sinha Ray and J. Bandyopadhyay, Role of Nanoclay Shape and Surface Characteristics on the Morphology and Thermal Properties of Polystyrene Nanocomposites Synthesized via Emulsion Polymerization, *Ind. Eng. Chem. Res.*, 2013, **52**, 16220–16231, DOI: **10.1021/ie4024929**.

53 M. L. Rahman, C. J. Fui, M. S. Sarjadi, S. E. Arshad, B. Musta, M. H. Abdullah and E. J. O'Reilly, Poly(amidoxime) ligand derived from waste palm fiber for the removal of heavy metals from electroplating wastewater, *Environ. Sci. Pollut. Res.*, 2020, **27**, 34541–34556, DOI: **10.1007/s11356-020-09462-0**.

54 Q. Ouyang, X. Wang, X. Wang, J. Huang, X. Huang and Y. Chen, Simultaneous DSC/TG analysis on the thermal behavior of PAN polymers prepared by aqueous free-radical polymerization, *Polym. Degrad. Stab.*, 2016, **130**, 320–327, DOI: **10.1016/j.polymdegradstab.2016.06.020**.

55 M. R. Lutfor, S. Silong, W. Md Zin, M. Z. Ab Rahman, M. Ahmad and J. Haron, Preparation and characterization of poly(amidoxime) chelating resin from polyacrylonitrile grafted sago starch, *Eur. Polym. J.*, 2000, **36**, 2105–2113, DOI: **10.1016/S0014-3057(99)00286-4**.

56 F. Altaf, *et al.*, Novel sepiolite reinforced emerging composite polymer electrolyte membranes for high-performance direct methanol fuel cells, *Mater. Today Chem.*, 2002, **24**, 100843, DOI: **10.1016/j.mtchem.2022.100843**.

57 F. Zhang, G. Huang, C. Hou, H. Wang, Q. Zhang and Y. Li, Polyacrylonitrile Fibers Anchored Cobalt/Graphene Sheet Nanocomposite: A Low-Cost, High-Performance and Reusable Catalyst for Hydrogen Generation, *J. Nanosci. Nanotechnol.*, 2016, **16**, 5627–5632, DOI: **10.1166/jnn.2016.11659**.

58 D. Shao, X. Liu, T. Hayat, J. Li and X. Ren, Poly(amidoxime) functionalized MoS$_2$ for efficient adsorption of uranium(VI) in aqueous solutions, *J. Radioanal. Nucl. Chem.*, 2019, **319**, 379–386, DOI: **10.1007/s10967-018-6338-7**.

59 G. Tartaglione, D. Tabuani and G. Camino, Thermal and morphological characterisation of organically modified sepiolite, *Microporous Mesoporous Mater.*, 2008, **107**, 161–168, DOI: **10.1016/j.micromeso.2007.04.020**.

60 A. Nasir, A. Raza, M. Tahir and T. Yasin, Free-radical graft polymerization of acrylonitrile on gamma irradiated graphene oxide: Synthesis and characterization, *Mater. Chem. Phys.*, 2020, **246**, 122807, DOI: **10.1016/j.matchemphys.2020.122807**.

61 M. Makaremi, R. T. De Silva and P. Pasbakhsh, Electrospun Nanofibrous Membranes of Polyacrylonitrile/Halloysite with Superior Water Filtration Ability, *J. Phys. Chem. C*, 2015, **119**, 7949–7958, DOI: **10.1021/acs.jpcc.5b00662**.

62 H. A. Abdelmonem, T. F. Hassanein, H. E. Sharafeldin, H. Gomaa, A. S. Ahmed, A. M. Abdel-lateef and A. H. Tilp, Cellulose-embedded polyacrylonitrile/amidoxime for the removal of cadmium(II) from wastewater: Adsorption performance and proposed mechanism, *Colloids Surf., A*, 2024, **684**, 133081, DOI: **10.1016/j.colsurfa.2023.133081**.

63 N. Berahim, W. Basirun, B. Leo and M. Johan, Synthesis of Bimetallic Gold–Silver (Au–Ag) Nanoparticles for the Catalytic Reduction of 4-Nitrophenol to 4-Aminophenol, *Catalysis*, 2018, **8**, 412, DOI: **10.3390/catal8100412**.

64 B. Vellaichamy and P. Periakaruppan, Silver nanoparticle-embedded RGO-nanosponge for superior catalytic activity towards 4-nitrophenol reduction, *RSC Adv.*, 2016, **6**, 88837–88845, DOI: **10.1039/C6RA19834A**.

65 Y.-C. Nie, F. Yu, L. C. Wang, Q. J. Xing, X. Liu, Y. Pei and S. L. Suib, Photocatalytic degradation of organic pollutants coupled with simultaneous photocatalytic H$_2$ evolution over graphene quantum dots/Mn-N-TiO$_2$/g-C$_3$N$_4$ composite catalysts: Performance and mechanism, *Appl. Catal., B*, 2018, **227**, 312–321, DOI: **10.1016/j.apcatb.2018.01.033**.

66 A. Iben Ayad, D. Luart, A. Ould Dris and E. Guénin, Kinetic Analysis of 4-Nitrophenol Reduction by 'Water-Soluble' Palladium Nanoparticles, *Nanomaterials*, 2020, **10**, 1169, DOI: **10.3390/nano10061169**.

67 J. W. Gregory, Y. Gong, Y. Han, S. Huband, R. I. Walton, V. Hessel and E. V. Rebrov, Au/TiO$_2$ coatings for photocatalytic reduction of 4-nitrophenol to 4-aminophenol with green light, *Catal. Today*, 2023, **418**, 114145, DOI: **10.1016/j.cattod.2023.114145**.

68 M. Bagheri, A. Melillo, B. Ferrer, M. Y. Masoomi and H. Garcia, Quasi-HKUST Prepared via Postsynthetic Defect Engineering for Highly Improved Catalytic Conversion of 4-Nitrophenol, *ACS Appl. Mater. Interfaces*, 2022, **14**, 978–989, DOI: **10.1021/acsami.1c19862**.

69 M. Wang, T. Shu, X. Ge, J. Hu and Y. Liang, Millimeter-Sized Hierarchical Porous Titanosilicate Supported Ultrafine Ag Nanoparticles as Highly Efficient Catalyst, *ChemistrySelect*, 2022, **7**, e202202260, DOI: **10.1002/slct.202202260**.

70 N. Pradhan, A. Pal and T. Pal, Silver nanoparticle catalyzed reduction of aromatic nitro compounds, *Colloids Surf., A*, 2002, **196**, 247–257, DOI: **10.1016/S0927-7757(01)01040-8**.

71 T. K. Das and N. C. Das, Advances on catalytic reduction of 4-nitrophenol by nanostructured materials as benchmark reaction, *Int. Nano Lett.*, 2022, **12**, 223–242, DOI: **10.1007/s40089-021-00362-w**.

72 M. Kohantorabi and M. R. Gholami, Kinetic Analysis of the Reduction of 4-Nitrophenol Catalyzed by CeO$_2$ Nanorods-Supported CuNi Nanoparticles, *Ind. Eng. Chem. Res.*, 2017, **56**, 1159–1167, DOI: **10.1021/acs.iecr.6b04208**.

73 M. Sharma, A. Mishra, A. Mehta, D. Choudhury and S. Basu, Enhanced catalytic and antibacterial activity of nanocasted mesoporous silver monoliths: kinetic and thermodynamic studies, *J. Sol-Gel Sci. Technol.*, 2017, **81**, 704–710, DOI: **10.1007/s10971-016-4260-4**.

74 N. E. Larm, D. V. Wagle, P. Ishtaweera, A. Roy and G. A. Baker, Surface Programmable Polycationic Nanoclay Supports Yielding 100 000 per Hour Turnover Frequencies for a Nanocatalyzed Canonical Nitroarene Reduction, *ACS Appl. Eng. Mater.*, 2023, **1**, 1913–1923, DOI: **10.1021/acsaenm.3c00243**.

75 Z. Yan, L. Fu, X. Zuo and H. Yang, Green assembly of stable and uniform silver nanoparticles on 2D silica nanosheets for catalytic reduction of 4-nitrophenol, *Appl. Catal., B*, 2018, **226**, 23–30, DOI: **10.1016/j.apcatb.2017.12.040**.

76 P. Zhang, Y. Sui, G. Xiao, Y. Wang, C. Wang, B. Liu and B. Zou, Facile fabrication of faceted copper nanocrystals with high catalytic activity for *p*-nitrophenol reduction, *J. Mater. Chem. A*, 2013, **1**, 1632–1638, DOI: **10.1039/C2TA00350C**.

77 M. E. Mahmoud, M. F. Amira, M. E. Abouelanwar and S. M. Seleim, Catalytic reduction of nitrophenols by a novel assembled nanocatalyst based on zerovalent copper-nanopolyaniline-nanozirconium silicate, *J. Mol. Liq.*, 2020, **299**, 112192, DOI: **10.1016/j.molliq.2019.112192**.

78 P. H. Zhang, Y. M. Sui, G. J. Xiao, Y. N. Wang, C. Z. Wang, B. B. Liu, G. T. Zou and B. Zou, Facile fabrication of faceted copper nanocrystals with high catalytic activity for *p*-nitrophenol reduction, *J. Mater. Chem. A*, 2013, **1**, 1632–1638, DOI: **10.1039/C2TA00350C**.

79 P. Deka, R. C. Deka and P. Bharali, In situ generated copper nanoparticle catalyzed reduction of 4-nitrophenol, *New J. Chem.*, 2014, **38**, 1789–1793, DOI: **10.1039/C3NJ01589K**.

80 F. M. Valadi and M. R. Gholami, Synthesis of CuCo2O4/BiVO4 composites as promise and efficient catalysts for 4-nitrophenol reduction in water: Experimental and theoretical study, *J. Environ. Chem. Eng.*, 2021, **9**, 105408, DOI: **10.1016/j.jece.2021.105408**.

81 X. Yang, H. Zhong, Y. Zhu, H. Jiang, J. Shen, J. Huang and C. Li, Highly efficient reusable catalyst based on silicon nanowire arrays decorated with copper nanoparticles, *J. Mater. Chem. A*, 2014, **2**, 9040–9047, DOI: **10.1039/C4TA00119B**.

82 Z. Wu, J. Zhu, W. Wen, X. Zhang and S. Wang, Spherical covalent organic framework supported Cu/Ag bimetallic nanoparticles with highly catalytic activity for reduction of 4-nitrophenol, *J. Solid State Chem.*, 2022, **311**, 123116, DOI: **10.1016/j.jssc.2022.123116**.

83 W. Jia, F. Tian, M. Zhang, X. Li, S. Ye, Y. Ma and J. Liu, Nitrogen-doped porous carbon-encapsulated copper composite for efficient reduction of 4-nitrophenol, *J. Colloid Interface Sci.*, 2021, **594**, 254–264, DOI: **10.1016/j.jcis.2021.03.020**.

84 X. Jiang, B. Han, C. Zhou, K. Xia, Q. Gao and J. Wu, Cu Nanoparticles Supported on Oxygen-Rich Boron Nitride for the Reduction of 4-Nitrophenol, *ACS Appl. Nano Mater.*, 2018, **1**, 6692–6700, DOI: **10.1021/acsanm.8b01506**.

85 Y. Sun, L. Xu, Z. Yin and X. Song, Synthesis of copper submicro/nanoplates with high stability and their recyclable superior catalytic activity towards 4-nitrophenol reduction, *J. Mater. Chem. A*, 2013, **1**, 12361–12370, DOI: **10.1039/C3TA12526B**.

86 A. A. Kassem, H. N. Abdelhamid, D. M. Fouad and S. A. Ibrahim, Catalytic reduction of 4-nitrophenol using copper terephthalate frameworks and CuO@C composite, *J. Environ. Chem. Eng.*, 2021, **9**, 104401, DOI: **10.1016/j.jece.2020.104401**.

87 H. Shin, S. Oh, H. Jun and M. Oh, Porous Composites Embedded With Cu and Co Nanoparticles for Efficient Catalytic Reduction of 4-Nitrophenol, *Bull. Korean Chem. Soc.*, 2021, **42**, 303–308, DOI: **10.1002/bkcs.12141**.

88 S. Gao, X. Jia, J. Yang and X. Wei, Hierarchically micro/nanostructured porous metallic copper: Convenient growth and superhydrophilic and catalytic performance, *J. Mater. Chem.*, 2012, **22**, 21733–21739, DOI: **10.1039/C2JM35233H**.

89 J. Jiang, G. H. Gunasekar, S. Park, S.-H. Kim, S. Yoon and L. Piao, Hierarchical Cu nanoparticle-aggregated cages with high catalytic activity for reduction of 4-nitrophenol and carbon dioxide, *Mater. Res. Bull.*, 2018, **100**, 184–190, DOI: **10.1016/j.materresbull.2017.12.018**.

90 Y. Sun, F. Zhang, L. Xu, Z. Yin and X. Song, Roughness-controlled copper nanowires and Cu nanowires–Ag heterostructures: synthesis and their enhanced catalysis, *J. Mater. Chem. A*, 2014, **2**, 18583–18592, DOI: **10.1039/C4TA03689A**.

91 X. Q. Wu, X. W. Wu, J. S. Shen and H. W. Zhang, In situ formed metal nanoparticle systems for catalytic reduction of nitroaromatic compounds, *RSC Adv.*, 2014, **4**, 49287–49294, DOI: **10.1039/C4RA07494G**.

92 T. Wi-Afedzi, E. Kwon, D. D. Tuan, K.-Y. A. Lin and F. Ghanbari, Copper hexacyanoferrate nanocrystal as a highly efficient non-noble metal catalyst for reduction of 4-nitrophenol in water, *Sci. Total Environ.*, 2019, **703**, 134781, DOI: **10.1016/j.scitotenv.2019.134781**.

93 P. Zhang, Y. Sui, G. Xiao, Y. Wang, C. Wang, B. Liu and B. Zou, Facile fabrication of faceted copper nanocrystals with high catalytic activity for *p*-nitrophenol reduction, *J. Mater. Chem. A*, 2013, **1**, 1632–1638, DOI: **10.1039/C2TA00350C**.

94 Y. Ma, *et al.*, N-doped carbon coated Mn3O4/PdCu nanocomposite as a high-performance catalyst for 4-nitrophenol reduction, *Sci. Total Environ.*, 2019, **696**, 134013, DOI: **10.1016/j.scitotenv.2019.134013**.